




RESEARCH ARTICLE | JANUARY 18 2024

Two potential paths for OH radical formation on surfaces of pure water microdroplets

Special Collection: [Water: Molecular Origins of its Anomalies](#)

Piotr Skurski ; Jack Simons  

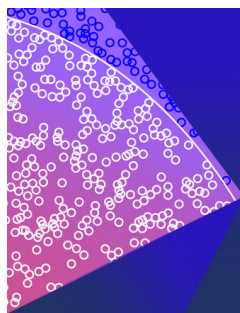


J. Chem. Phys. 160, 034708 (2024)

<https://doi.org/10.1063/5.0188908>



CrossMark



The Journal of Chemical Physics

Special Topic: Monte Carlo methods,
70 years after Metropolis *et al.* (1953)

Submit Today

Two potential paths for OH radical formation on surfaces of pure water microdroplets

Cite as: J. Chem. Phys. 160, 034708 (2024); doi: 10.1063/5.0188908

Submitted: 24 November 2023 • Accepted: 27 December 2023 •

Published Online: 18 January 2024



Piotr Skurski^{1,2} and Jack Simons^{1,a)}

AFFILIATIONS

¹ Henry Eyring Center for Theoretical Chemistry, Department of Chemistry, University of Utah, Salt Lake City, Utah 84112, USA

² Laboratory of Quantum Chemistry, Faculty of Chemistry, University of Gdańsk, Wita Stwosza 63, 80-308 Gdańsk, Poland

Note: This paper is part of the JCP Special Topic on Water: Molecular Origins of its Anomalies.

a) Author to whom correspondence should be addressed: jack.simons@utah.edu

ABSTRACT

Experimental findings by others suggest that OH radicals are formed in unexpected abundance on or near surfaces of 1–50 μm microdroplets comprised of pure water, but the mechanism by which these radicals are generated is not yet fully resolved. In this work, we examine two possibilities using *ab initio* electronic structure methods: (1) electron transfer (ET) from a microdroplet surface-bound OH^- anion to a nearby H_3O^+ cation and (2) proton transfer (PT) from such a H_3O^+ cation to a nearby OH^- anion. Our findings suggest that both processes are possible but only if the droplet's underlying water molecules comprising the microdroplet provide little screening of the Coulomb interaction between the anion and cation once they reach ~ 10 Å of one another. In the ET event, an OH radical is formed directly; for PT, the OH formation occurs because the new O–H bond formed by the transferred proton is created at a bond length sufficiently elongated to permit homolytic cleavage. Both the ET and PT pathways predict that H atoms will also be formed. Finally, we discuss the roles played by strong local electric fields in mechanisms that have previously been proposed and that occur in our two mechanisms.

Published under an exclusive license by AIP Publishing. <https://doi.org/10.1063/5.0188908>

I. INTRODUCTION

In this paper, we have studied what can happen when an OH^- anion and an H_3O^+ cation recombine to form a water dimer (H_2O_2). The novel aspects of this study involve considering the possibilities that an encounter between these ions might result in electron transfer to generate an OH radical and a H_3O Rydberg radical and/or proton transfer involving collisions with sufficient kinetic energy to fragment the water dimer into $\text{H}_2\text{O}(\text{OH}) + \text{H}$. In both reactions, OH radicals can be formed. Before explaining the methods we employed and discussing our findings, we want to let you know what motivated us to explore these possibilities.

A. Motivation

Dick Zare's group^{1,2} reported that H_2O_2 appears to be formed from microdroplets of water with diameters in the 1–50 μm range with higher local concentrations of H_2O_2 generated in smaller droplets than in larger droplets, suggesting that the generation of H_2O_2 occurs near the surface of the droplet. Those researchers proposed it was likely OH^- anions residing near the surface of the

droplets that were operative and suggested that OH radicals produced from detaching an electron from OH^- anions were reacting to generate H_2O_2 .

The Zare group proposed that OH^- ions near the surface are more susceptible than OH^- anions in the bulk to losing an electron to generate OH radicals. We know that in the bulk, it takes about 3.5 eV to detach an electron from OH^- , but it still takes 1.83 eV to detach an electron from an isolated OH^- ion. Zare *et al.* suggested that strong local electric fields, which had been shown to occur at or near the interface,^{3,4} might facilitate detachment of an electron from OH^- to generate an OH radical and a free electron, but they noted that they did not know where the detached electron then goes. This seems plausible to us, but we thought of two other options that we decided to explore, both of which account for the fate of all the electrons.

It is with these experimental findings in mind that we undertook this study in which we examined the electronic energy surfaces that would govern two reactions $\text{OH}^- + \text{H}_3\text{O}^+ \rightarrow \text{H}_2\text{O} \cdots \text{H}_2\text{O}$ and $\text{OH}^- + \text{H}_3\text{O}^+ \rightarrow \text{HO} + \text{H}_3\text{O}$, either of which could generate the OH radicals postulated to produce H_2O_2 . In the latter reaction, OH is

a primary product, and the fragile H_3O Rydberg radical would be expected to dissociate to produce H atoms and H_2O . In the former reaction, if the final encounter of the cation and anion were sufficiently energetic, as we show to likely be the case, the nascent $\text{H}_2\text{O} \cdots \text{H}_2\text{O}$ water dimer could fragment into $\text{H} + \text{H}_2\text{O} \cdots \text{OH}$ and, thus, provide a source of the OH radicals.

These two reaction pathways involve electron transfer and proton transfer. In this study, we examine them both treating the anion–cation encounter in the absence of any solvation and treating it with solvation modeled using a continuum solvation model. We wish to emphasize that such approximate treatment of surface solvation effects should not be expected to provide quantitatively accurate predictions. However, we do think that our work provides a route toward suggesting whether either of the two reaction pathways could be feasible for OH^- and H_3O^+ ions existing on the liquid/vapor water interface. Before proceeding further, we think it is appropriate to justify our approach in a bit more detail.

In 2001, Geissler *et al.*⁵ studied the autoionization of liquid water to generate OH^- and H_3O^+ using *ab initio* molecular dynamics simulations. Because the autoionization is an extremely rare event, they employed a specialized transition path sampling technique to simulate the surrounding solvent's (rare) fluctuations that are needed to bring three water molecules into what they termed a hydrogen-bond “wire” geometry. Upon reaching this critical geometry, a proton transfer along the wire within the three water molecules occurs to generate the ion-pair products. These products have some chance to diffuse apart, but most of the time they recombine to reform the neutral water trimer wire. We will provide a bit more detail about this study later when we discuss our results.

Subsequently, Hassanali *et al.*⁶ studied the recombination of H_3O^+ and OH^- in water again focusing on “wire” structures within which the ultimate proton transfer step occurs. They found two time scales to be relevant: one (~ 0.5 ps) in which the electric fields generated by the surrounding solvent compress a small number of water molecules into a wire geometry that allows the proton transfer to begin and the second (~ 65 fs) relates to how long it takes the proton transfer step to occur within the wire.

It should be noted in both of the studies just discussed that it was only the behavior of the water molecules involved in the proton transfer process once they were within ~ 10 Å of one another that was incorporated. They did not explicitly include the diffusive motions of the OH^- and H_3O^+ ions away from or toward one another after or prior to the proton transfer event because such motions take place on timescales well outside the range of their simulations.

In our study, we also focus primarily on what happens when the OH^- and H_3O^+ ions on a microdroplet's surface are within ~ 10 Å, not as they undergo Grotthuss proton transfers or diffuse or hop from site to site. We do not use the same three-water wire model as employed in Refs. 5 and 6. Instead, we consider the encounter of a single OH^- ion with a single H_3O^+ ion once they have come within ~ 10 Å of one another on the microdroplet's surface. We do so either in the absence of any representation of the droplet's surface solvation effect by using a continuum polarization model to simulate these effects.

We are attempting to model the behavior of OH^- and H_3O^+ ions residing on the surface of the microdroplet where they are attached to solvent water molecules from below (i.e., inward toward the bulk liquid). Moreover, as explained above, we do so only once

the ions have come within ~ 10 Å of one another. We view the surface-translational movement of these ions as occurring by their being temporarily detached from the underlying solvent molecules, allowing them to hop a short distance (< 10 Å) to another binding site, ultimately reaching critical distances at which an electron or proton transfer can occur. As we discuss later, their detachment from a binding site could occur thermally (N.B., at 298 K⁰, $kT = 0.026$ eV = 0.6 kcal/mol) or could be assisted by the Coulomb attraction potential -14.4 eV Å/[$\epsilon R(\text{Å})$] between the two ions, where the dielectric constant ϵ is used to model any screening that might be present and $R(\text{Å})$ is the distance in Å between the anion and cation.

For a cation/ion pair that has migrated to such a critical distance, the underlying solvent molecules might, of course, have an effect on their mutual interaction energy. In our study, we attempt to address this issue not in a manner to achieve accurate predictive reaction rates. Instead, we are trying to explore whether either of the two reaction pathways we present here could be plausible explanations for the source of OH radicals that seem to be formed in the Zare-lab experiments. Therefore, we explore the electronic energy surfaces relevant to the two reactions in three cases: in the absence of any dielectric screening, with screening to model the high-frequency dielectric response ($\epsilon = 2$) of the water solvent, and with screening to model water solvent's full dielectric response ($\epsilon = 78$). For one OH^- anion and one H_3O^+ cation within ~ 10 Å, there may be few or no H_2O molecules immediately between them on the surface, but there will be numerous H_2O molecules below and to the sides of them in the underlying liquid of the droplet. If the electron transfer or proton transfer event is very fast, the underlying solvent may only have time to exert its high-frequency screening. On the other hand, if either of these transfer processes is slow, the full screening could be more appropriate. This illustrates how we view the results thus obtained as limiting-case estimates whose value mainly offers guidance for what mechanisms are plausible.

B. Outline of our study

In Sec. II, we detail the computational methods employed in our study. In Sec. III, we first provide and discuss the results of our electron transfer calculations and then do likewise for our proton transfer study. In Sec. IV, we reflect on what our findings say and suggest about the experimental findings reported in Refs. 1 and 2.

II. METHODS

The equilibrium structure and the corresponding harmonic vibrational frequencies of the isolated neutral $(\text{H}_2\text{O})_2$ water dimer were determined by applying the second-order Møller–Plesset (MP2) perturbation method^{7–9} with the aug-cc-pVDZ¹⁰ basis set supplemented with 3s3p sets of diffuse functions centered on both oxygen atoms. The extra diffuse functions do not share exponent values, and we used even-tempered¹¹ three-term *s* and three-term *p* basis sets. The geometric progression ratio was equal to 3.2,¹² and for each symmetry, we started to build up the exponents of the extra diffuse functions from the lowest exponent of the same symmetry included in the aug-cc-pVDZ basis set designed for oxygen. As a consequence, we achieved lowest exponents of 2.4097×10^{-3} and 2.0923×10^{-3} a.u. for the *s* and *p* symmetries, respectively.

We examined the lowest eigenvalue of the atomic orbital overlap matrix to determine that near linear dependency was not a problem.

The relaxed scans of the potential energy surfaces [i.e., partial geometry optimizations assuming a certain interatomic separation (either oxygen–oxygen or oxygen–hydrogen) frozen and the other bond lengths and angles relaxed to minimize the energy] were performed at the same MP2/aug-cc-pVDZ + 3s3p theory level.

The avoided crossings between the $\text{OH}\cdots\text{H}_3\text{O}$ and $\text{OH}^-\cdots\text{H}_3\text{O}^+$ energy profiles (representing the two singlet states) for the oxygen–oxygen separations near the crossing points were studied by using the complete active space multiconfiguration SCF procedure^{13–18} involving four electrons and a subset of four

orbitals in the active space [i.e., CAS-SCF(4,4)] with an MP2-level electron correlation correction¹⁹ to the CAS-SCF energy. The diabatic energy profiles describing the heterolytic and homolytic dissociation of the water dimer into either $\text{H}_2\text{O}(\text{OH}^-) + \text{H}^+$ or $(\text{OH})\text{H}_2\text{O} + \text{H}$ were determined likewise [by employing the CAS-SCF(4,4) technique together with the MP2-level correction]. In all CAS-SCF calculations, the aug-cc-pVDZ + 3s3p basis set was used. This particular active space was selected so that all of the following orbital occupancies could be accommodated: (i) the closed-shell situation in $(\text{H}_2\text{O})_2$, (ii) the doubly open-shell situation in $(\text{H}_2\text{O})\text{OH} + \text{H}$, (iii) the closed-shell situation in $(\text{H}_2\text{O})\text{OH}^- + \text{H}^+$, (iv) the doubly open-shell situation in $\text{OH} + \text{H}_3\text{O}$, and (v) the closed-shell situation in $\text{OH}^- + \text{H}_3\text{O}^+$. In all cases, we examined

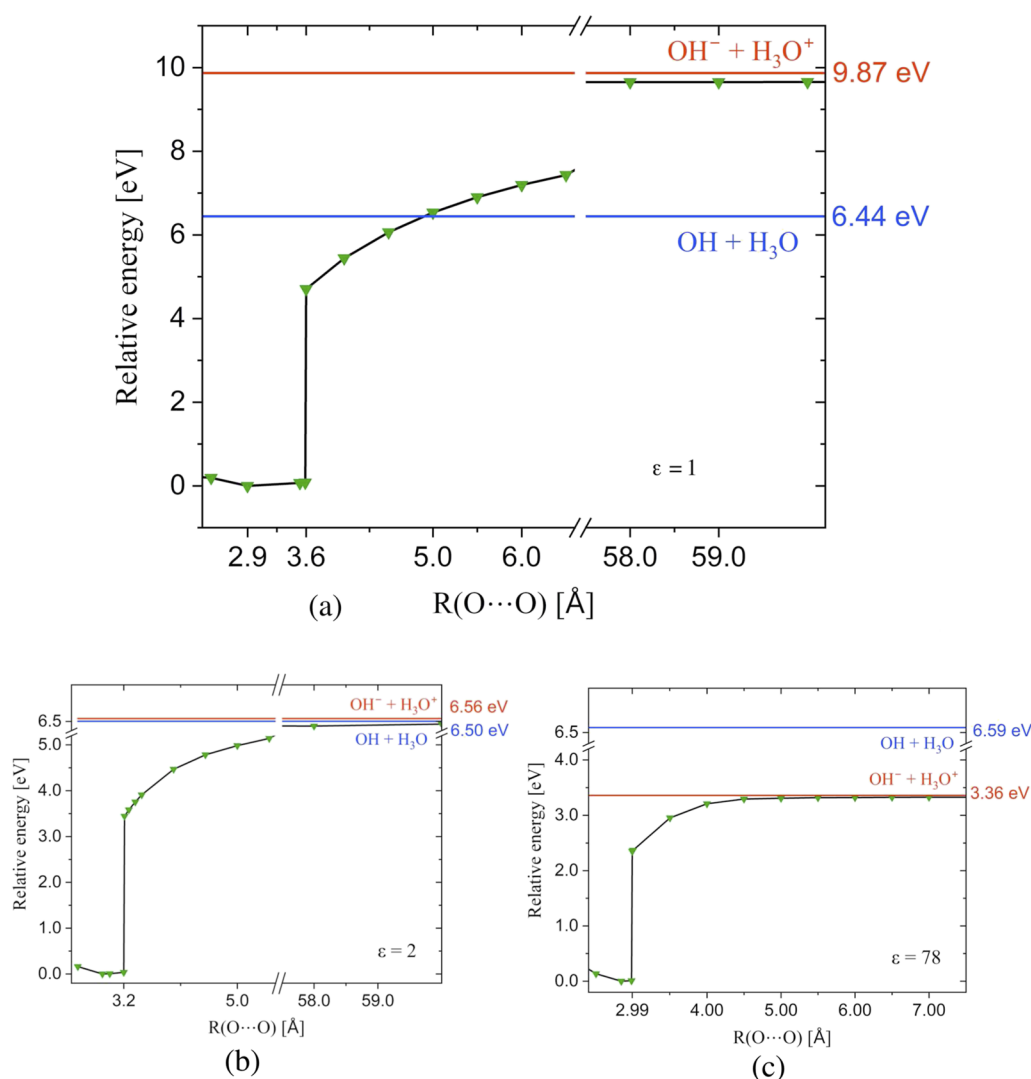


FIG. 1. Energies of $\text{OH}^-\cdots\text{H}_3\text{O}^+$ (green) as a function of the O–O distance with all other coordinates relaxed to minimize the energy for $\epsilon = 1$ (a), 2 (b), and 78 (c). In blue is shown the asymptotic energy of $\text{OH} + \text{H}_3\text{O}$ and in red is the asymptotic energy of $\text{OH}^- + \text{H}_3\text{O}^+$.

the resultant occupied molecular orbitals to assure that they had the desired character.

The solvent effects were approximated by employing the polarized continuum solvation model (PCM)^{20–22} within a self-consistent reaction field treatment, as implemented in the GAUSSIAN16 package [the default options for PCM and dielectric constants (ϵ) of 2 and 78 were used]. All calculations were performed with the GAUSSIAN16 (Rev. C.01) program suite.²³

III. RESULTS

A. Overview of reaction energy profiles

In Fig. 1, we show plots of the relative energies of the reactants and products in the proton-transfer (PT) and electron-transfer (ET) reactions with the screening from the surrounding water treated using PCM dielectric constants of 1, 2, and 78. All energies are shown relative to that of the water dimer at its equilibrium geometry. At each distance R_{OO} between the two oxygen atoms, the other bond lengths and angles have been “relaxed” to minimize the energy unless specified otherwise. As stated earlier, it is more likely that the two ions undergo Grotthuss, diffusion, or hopping movements along and on-and-off the surface. However, once they come within ~ 10 Å of one another, we think that the energy profiles in Fig. 1 can be quite relevant as a way of thinking about what might occur if the underlying droplet surface has no additional effects.

We first wish to point out a few key features of the data shown in Fig. 1(a). The energy profile for the $\text{OH}^- \cdots \text{H}_3\text{O}^+$ ion pair follows, at large R_{OO} , the functional form $9.87 \text{ eV} - 14.4 \text{ eV } \text{\AA}/R_{OO}(\text{\AA})$ expected for the two ions whose energy lies 9.87 eV above that of the water dimer at large R_{OO} and decreases according to an unscreened Coulomb attraction. Second, the energy profile of the $\text{OH} \cdots \text{H}_3\text{O}$ radical pair varies little with R_{OO} and is shown to lie 6.44 eV above the water dimer at large R_{OO} . Later, when we address the details of the coupling between the ion-pair and radical-pair curves, we will

show more precise data for both curves computed for a range of R_{OO} values near the crossing at the relaxed geometry of the ion pair. In those calculations, a common geometry is employed because the ET process is initiated at the ion-pair geometry and occurs faster than the radical-pair formed has time to undergo geometrical relaxation. Third, the radical-pair and ion-pair curves appear to intersect near $R_{OO} = 5.0$ Å; this is where the ET event might take place as we discuss in detail later and where we will provide a more precise value for where an actual avoided crossing occurs. Fourth, the ion-pair curve undergoes a steep drop of ~ 4.74 eV near $R_{OO} = 3.6$ Å; as we show later, this is where the PT takes place to form the water dimer.

We show in Figs. 1(b) and 1(c) plots analogous to those in Fig. 1(a), including/approximating solvation effects in terms of a continuum dielectric constant of $\epsilon = 2$ and $\epsilon = 78$, respectively. There are a few things to notice in Figs. 1(b) and 1(c) when compared to Fig. 1(a). First, for $\epsilon = 2$, the $\text{OH}^- \cdots \text{H}_3\text{O}^+$ and $\text{OH} \cdots \text{H}_3\text{O}$ curves still have a crossing, but it occurs at a much longer R_{OO} than for $\epsilon = 1$; for $\epsilon = 78$, the $\text{OH} \cdots \text{H}_3\text{O}$ curve remains far above the $\text{OH}^- \cdots \text{H}_3\text{O}^+$ curve at all distances, so there is no crossing. These data suggest that ET might be operative but only if the microdroplet's environment is very weakly solvating (e.g., consistent with $\epsilon = 2$ or lower). Second, although the R_{OO} value at which the ion-pair curve undergoes a sudden drop is a bit smaller for $\epsilon = 2$ and $\epsilon = 78$ than for $\epsilon = 1$, the energy-drops' magnitudes are quite different; for $\epsilon = 1$, the drop is 4.75 eV, and for $\epsilon = 2$ and $\epsilon = 78$, they are 3.5 and 2.4 eV, respectively. These changes in the energy drop will be shown later to play key roles in deciding whether PT can be a source of OH radical formation.

Before moving on to discuss the possibility of ET, we want to further clarify what is happening in the regions of steep drops shown in Fig. 1 by demonstrating that the reaction energy profiles illustrated in the steep-drop regions are good representations of the corresponding intrinsic reaction coordinate (IRC) profiles. The IRC is defined as the minimum energy reaction pathway in

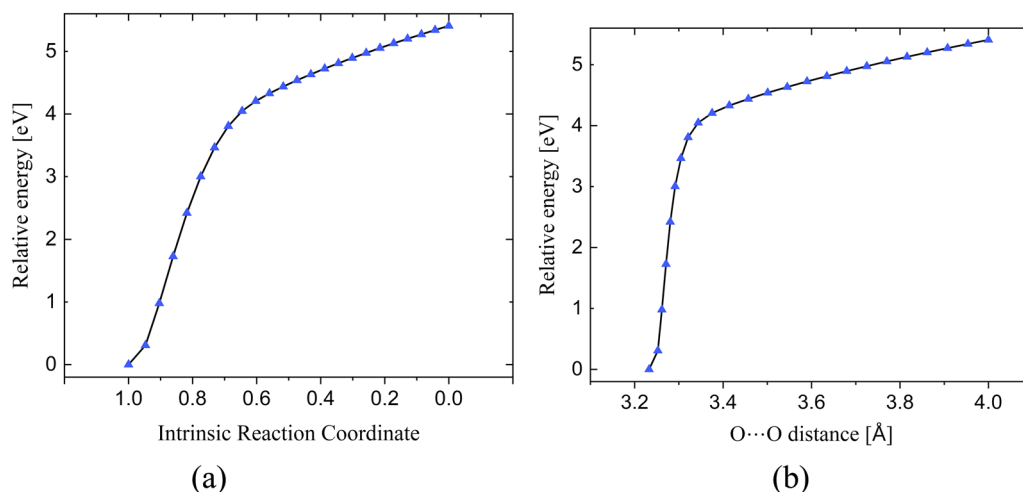


FIG. 2. Energies of $\text{OH}^- \cdots \text{H}_3\text{O}^+$ along the intrinsic reaction coordinate (a) starting at $R_{OO} = 4.0$ Å and leading to the equilibrium geometry of the water dimer; energies along this same path plotted as functions of the O–O distance (b).

mass-weighted Cartesian coordinates between the chosen stage of a reaction and its final product. In our case in which we proceed downhill to the water dimer minimum, it traces out a path parallel to the local gradient starting at a point where this gradient lies along the negative Hessian eigenvalue's eigenvector. In mapping out the energy profile associated with the IRC associated with Fig. 1(a), we utilized the Gonzalez–Schlegel method.²⁴

For the case shown in Fig. 1(a), we carried out such an IRC study beginning at an R_{OO} value of 4 Å and we followed the IRC downward in energy to the water-dimer product geometry. The energy variation along this IRC is shown in Fig. 2(a). At each point along this IRC, we measured the R_{OO} value; this allowed us to make a plot of energy vs R_{OO} for points actually lying on the IRC. The data for this plot are shown in Fig. 2(b).

This test shows that the behavior of the energies shown in Fig. 1 where steep drops occur is indeed properly representative of the actual IRC energy profiles in these regions. As we show later, it is in these regions that a proton is transferred from H_3O^+ to OH^- , and the magnitudes of the energy drops play key roles in determining whether the PT mechanism can generate OH radicals.

B. Electron transfer pathway

To determine whether it is feasible to suggest that the ET path, which generates $OH + H_3O$, is feasible, we had to examine the avoided crossing between the $OH \cdots H_3O$ and $OH^- \cdots H_3O^+$ curves. As explained in Sec. II, we used a CAS-SCF procedure to calculate the energies of these two singlet states for R_{OO} values near the suggested crossing points shown in Fig. 1. Both the ion-pair and radical-pair energies were computed, for each R_{OO} , at the relaxed geometry of the ion pair because this is the geometry at which the ET is initiated. In Fig. 3, we show these energy plots for $\epsilon = 1$ and $\epsilon = 2$ (recall, no crossing occurs for $\epsilon = 78$).

Because the $HO^- \cdots H_3O^+$ and $HO \cdots H_3O$ states are of the same spatial and spin symmetries, they undergo an avoided crossing whose magnitude (i.e., the minimum energy gap) reflects the electronic coupling between the OH^- ion's p_π orbital and the H_3O

radical's Rydberg orbital that are involved in the ET event. Clearly, the coupling strength, as contained in the minimum energy gaps shown in Fig. 3, between these two states is much smaller for $\epsilon = 2$ than for $\epsilon = 1$.

To estimate the probability P of ET for each of these cases, we make use of Landau–Zener theory,²⁵ which approximates the probability as $P = \frac{2\pi H^2}{\hbar v | \frac{dE_1}{dR} - \frac{dE_2}{dR} |}$. Here, H is the magnitude in the coupling between the two states (determined as $1/2$ the minimum splitting between the pairs of curves shown in Fig. 3), and v is the speed at which the two ions pass through the crossing point. $| \frac{dE_1}{dR} - \frac{dE_2}{dR} |$ is the difference in the slopes of the two curves as they approach the avoided crossing. This expression for the ET probability can be recast in units of eV for energies and Å for distances as $P = \frac{68.7 |H_{eV}|^2}{\sqrt{\frac{KE_{eV}}{\mu_{amu}} | \frac{dE_1}{dR} - \frac{dE_2}{dR} |_{eV/\text{Å}}}}$, where μ is the reduced mass of the $OH^- \cdots H_3O^+$ pair in atomic mass units. Estimating the slopes as in Fig. 3 and employing the H energy gaps reported there and inserting $17 \times 19/36$ as the reduced mass, these probabilities turn out to be $P = 0.11(KE)^{-1/2}$ and $P = 5 \times 10^{-5}(KE)^{-1/2}$, respectively.

It is difficult to know what values are appropriate to use for the kinetic energy with which the ion pair enters the avoided crossing. For $\epsilon = 2$, it seems reasonable to estimate KE either in terms of a thermal value or by the energy drop the ion-pair state undergoes as it evolves from its asymptote to the crossing. At 298 K⁰, $KE = 0.026$ eV, so $(KE)^{-1/2} = 6.2$. Alternatively, using the energy drop [see Fig. 1(b)] of $6.56 - 6.50 = 0.06$ eV, one obtains $(KE)^{-1/2} = 4.1$. In either case, the probability $P = 5 \times 10^{-5}(KE)^{-1/2}$ turns out to be very small. This suggests that if the underlying solvent provides screening consistent with the high-frequency dielectric or more, ET is not to be expected as a pathway to OH formation.

On the other hand, if the situation is more realistically described by the $\epsilon = 1$ model whose results appear in Figs. 1(a) and 3(a), our predictions are different. Again estimating the kinetic energy as thermal [$(KE)^{-1/2} = 6.2$], the ET probability $P = 0.11(KE)^{-1/2}$ turns out to be 0.68. An upper limit to KE can

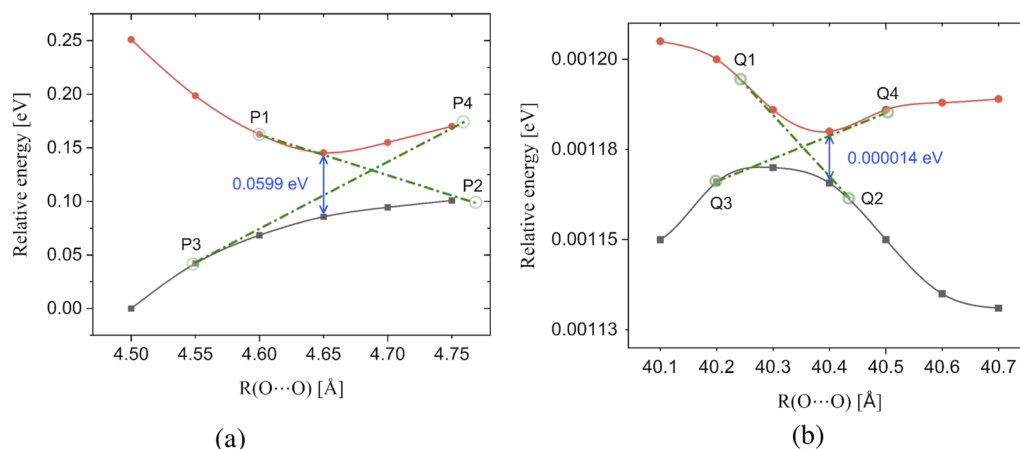


FIG. 3. Energies of the adiabatic $HO^- \cdots H_3O^+/HO \cdots H_3O$ states near their avoided crossing for $\epsilon = 1$ (a) and $\epsilon = 2$ (b), showing the minimum energy gap and the points used to estimate the slopes.

be obtained by assuming that the ion-pair retains its full Coulomb energy drop of $9.87 - 6.44 = 3.23$ eV [see Fig. 1(a)] as it evolves from large R_{OO} to the crossing point. In this case, the ET probability $P = 0.11(KE)^{-1/2}$ turns out to be 0.06. It seems highly unlikely that the ion-pair would evolve unhindered over large distances as the latter estimate assumes. Hence, we are more inclined to make an estimate using the lower KE value. This would suggest that if the underlying solvent had little or no dielectric screening effect on the ion-pair encounter, there should be a good chance of an ET event, which could then be a source of OH radicals. It is useful to note that in this case, H atoms should also be formed, an outcome that could be subjected to experimental test.

C. Proton transfer pathway

As an introduction to how we attempt to simulate the PT pathway, in Fig. 4, we show a depiction taken from Ref. 5 that was used to describe the PT process involved in the reverse process: forming OH^- and H_3O^+ from water. The picture of the PT reaction put forth in Ref. 5 is quite similar to that contained in the well-known Marcus theory. In both, it is a collective reorganization of many surrounding solvent molecules that gives rise to a change in the local potential energy landscape experienced by the proton to be transferred. These collective geometrical displacements involve many solvent molecules, which precludes focusing on one or a few molecular coordinates to define some kind of intrinsic reaction path. In the Marcus theory, a solvent reorganization coordinate is introduced, while in Ref. 5, a coordinate q that interpolates between geometries representative of $\text{OH}^- \cdots \text{OH}_2$ and $\text{OH}_2 \cdots \text{OH}_2$ is introduced.

In Fig. 4, the potential energy landscape experienced by the proton to be transferred is shown as a function of a coordinate q measuring the extent of transfer. In the top picture, there is a potential minimum at $q = 1$, which describes the water wire in its $(\text{H}_2\text{O})_3$ water-trimer state. The $\text{H}_3\text{O}^+ \cdots \text{H}_2\text{O} \cdots \text{OH}^-$ species is depicted at the left where $q = 0$ and where there is no minimum in the energy profile. This is a picture of the energy landscape discovered during the molecular dynamics simulation of Ref. 5 and reflects one situation of the solvent's internal electric fields. In the middle and bottom pictures, which relate to two other situations of the solvent's electric fields, the energy profile is shown (middle) evolving into one having minima at both $q = 1$ and $q = 0$ but with the water trimer being lower and subsequently (bottom) into a profile in which the $\text{H}_3\text{O}^+ \cdots \text{H}_2\text{O} \cdots \text{OH}^-$ minimum is lower than the water trimer minimum. The evolution in the transferred proton's energy profile was induced through changes in the surrounding water solvent molecules' electric fields taking place during the molecular dynamics simulation.

In our case, the proton to be transferred also exists in a landscape that has two minima: one in which it is bound within the H_3O^+ ion and the other when it transfers from H_3O^+ to the OH^- ion to reside within $(\text{H}_2\text{O})_2$. In Fig. 5, we illustrate (for now qualitatively) the two local minima when the two ions are far apart by the two black potential energy profiles $V(R(\text{H}-\text{O}_L))$ and $V(R(\text{H}-\text{O}_R))$. In $V(R(\text{H}-\text{O}_L))$, the proton is bound to the oxygen atom on the left (hence the label L) within the water dimer. In $V(R(\text{H}-\text{O}_R))$, it is bound to the oxygen atom on the right within H_3O^+ .

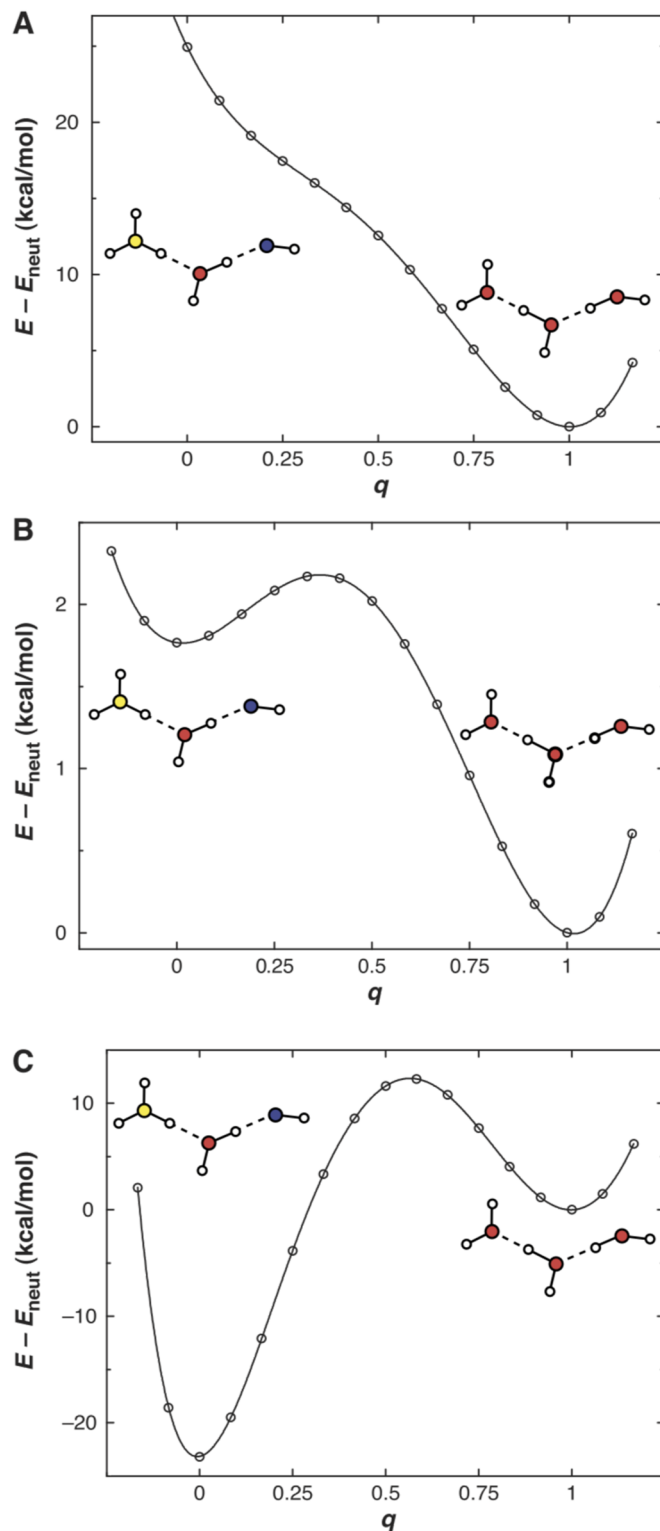


FIG. 4. Energies of the $\text{H}_3\text{O}^+ \cdots \text{H}_2\text{O} \cdots \text{OH}^-$ (left) and $(\text{H}_2\text{O})_3$ (right) structures as functions of a PT reaction progress variable q for three values of the solvent's local electric field (top to bottom).

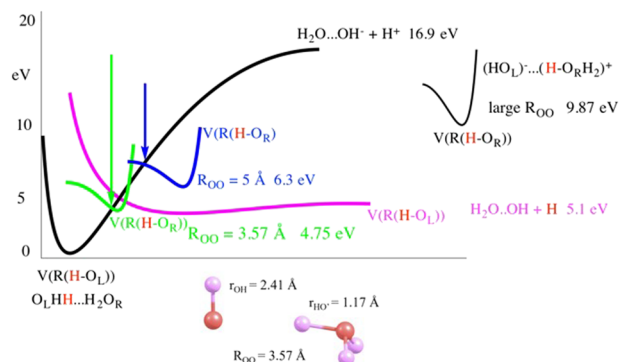


FIG. 5. Qualitative depiction of local minima holding the transferred proton within the water dimer (black curve on left) and within the $\text{OH}^- \cdots \text{H}_3\text{O}^+$ ion pair (black curve on right). In blue and green, the ion-pair curve is duplicated as the two ions move closer (to $R_{\text{OO}} = 5 \text{ \AA}$ and $R_{\text{OO}} = 3.57 \text{ \AA}$). The presence of an activation barrier at $R_{\text{OO}} = 5$ is indicated by the blue arrow, and the absence of a barrier at $R_{\text{OO}} = 3.57 \text{ \AA}$ is indicated by the green arrow. The fucia curve represents the homolytic cleavage profile leading from the water dimer to H atoms and a $\text{H}_2\text{O} \cdots \text{OH}$ radical complex.

Unlike the situation described earlier in which it was evolution of the electric fields from the surrounding bulk water that induced the evolution of the energy landscape, in our case, it is the evolution of the stabilizing Coulomb potential arising from movement of the anion and cation toward one another, as also suggested in Fig. 5 by the black, blue, and green $V(R(\text{H}-\text{O}_R))$ profiles. Figure 5 also contains in fucia a potential that relates to the homolytic cleavage of an O–H bond within the water dimer; its importance will be discussed after we conclude our discussion of the PT process.

At very large R_{OO} (top right), the proton to be transferred (red) is bound within H_3O^+ , and the variation in its energy as its O–H bond length is stretched is colored black and denoted $V(R(\text{H}-\text{O}_R))$, where O_R denotes the oxygen atom on the right where H_3O^+ exists. As the two ions approach one another, the ion-pair state's minimum and potential profile decrease in energy due to the attractive Coulomb interaction between the two ions. For example, at the intermediate R_{OO} distance of 5 \AA , there remains an activation barrier (blue arrow), a proton on H_3O^+ must overcome to reach the black water-dimer potential $V(R(\text{H}-\text{O}_L))$; that is, PT is an activated process under these conditions. As the two ions approach even closer, they reach a R_{OO} value of 3.57 \AA at which the minimum on the $V(R(\text{H}-\text{O}_R))$ branch of the energy surface intersects the water dimer branch (green arrow). At this critical distance, the PT can occur with zero activation energy, and this is where steep drop off seen in Fig. 1(a) takes place. The lack of an activation energy should not be surprising as it also occurs in Marcus theory when the minimum of one Marcus parabola intersects the other parabola whose minimum lies at a lower energy.

Further examining what happens in the steep drop regions, in Fig. 6, we show for $\epsilon = 1$ the geometry of $\text{OH}^- \cdots \text{H}_3\text{O}^+$ at $R_{\text{OO}} = 5.00 \text{ \AA}$ at the top [far away from the steep drop as can be seen in Fig. 1(a)] and at $R_{\text{OO}} = 3.57 \text{ \AA}$ in the middle (just prior to the steep drop). At these two geometries, the proton to be transferred is still attached within the H_3O^+ unit and has an associated bond length that is less than 0.2 \AA longer than in isolated H_3O^+ (0.98 \AA). Then,

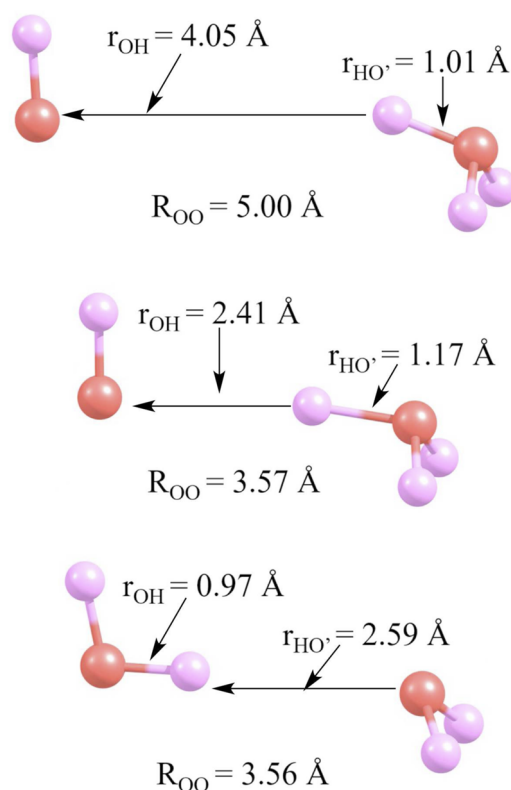


FIG. 6. Geometries of the two fragments at three values of the O–O distance illustrating the sudden change between $R_{\text{OO}} = 3.57 \text{ \AA}$ and $R_{\text{OO}} = 3.56 \text{ \AA}$.

suddenly, at $R_{\text{OO}} = 3.56 \text{ \AA}$, the proton has moved onto the OH^- site to form an intact H_2O where its bond length (0.97 \AA) is very close to that within the water dimer.

There are two important observations we want to emphasize about the structures shown in Fig. 6. First, at long R_{OO} values and even just prior to the PT event, the proton to be transferred is bound to the H_3O^+ unit within a very narrow range of bond lengths near the equilibrium length in H_3O^+ (0.98 \AA). This observation allows us to think of the position of the active proton at all times prior to PT as near the minimum of the black, blue, and green $V(R(\text{H}-\text{O}_R))$ curves shown in Fig. 5. Second, just prior to PT, the active proton resides 2.41 \AA away from the HO^- anion's oxygen atom labeled O_L , which is quite far from its equilibrium distance after PT when this proton resides within the water dimer (0.97 \AA). This allows us to position the curve crossing between the green $V(R(\text{H}-\text{O}_R))$ and black $V(R(\text{H}-\text{O}_L))$ curves in Fig. 5 at an extended bond length within the black water-dimer $V(R(\text{H}-\text{O}_L))$ curve on the left in Fig. 5. This, in turn, is the origin of our claim that the water dimer formed by PT will possess significant vibrational energy in the newly formed O–H bond.

Now, it is time to discuss the role of the fucia energy profile shown in Fig. 5. The black $V(R(\text{H}-\text{O}_L))$ and fucia $V(R(\text{H}-\text{O}_L))$ curves shown there represent diabatic energy profiles describing heterolytic and homolytic dissociation of the water dimer into

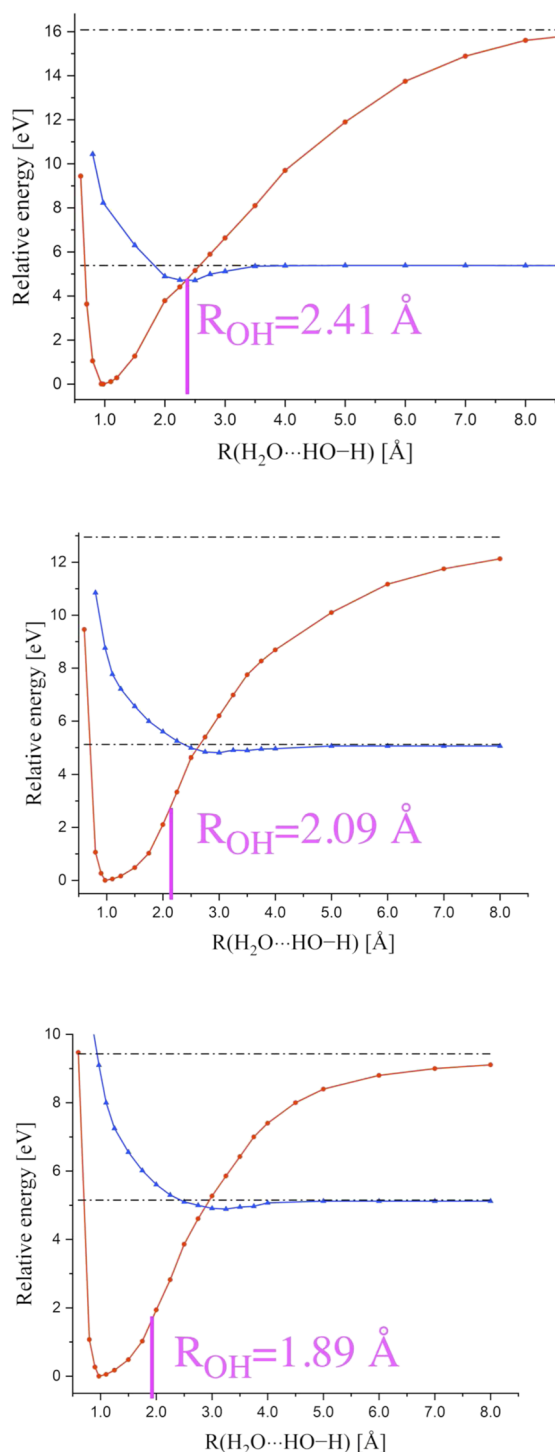


FIG. 7. Quantitative plots for $\epsilon = 1, 2$, and 78 (top to bottom) of the diabatic heterolytic (red) and homolytic (blue) dissociations discussed in the text as functions of the length $R(\text{OH}_2 \cdots \text{HO-H})$ of one O-H bond that is broken with all other degrees of freedom relaxed to minimize the energy. In fucia is shown the distance R_{OH} from the transferred proton to the OH^- anion's oxygen atom at the steep energy drop in Fig. 1.

$\text{H}_2\text{O}(\text{OH}^-) + \text{H}^+$ or into $\text{H}_2\text{O}(\text{OH}) + \text{H}$, respectively. The mechanistic picture described above suggests that the PT event generates a water dimer structure $\text{OHH} \cdots \text{OH}_2$ in which the newly formed O-H bond is quite elongated and resides on the left oxygen atom. In now considering the homolytic cleavage of this dimer to form H atoms and $\text{OH} \cdots \text{OH}_2$ radicals, it is by no means clear which O-H bond might undergo cleavage. It may well be that intramolecular vibrational energy transfer takes place between the nascent O-H bond and other O-H bonds in the dimer. Regardless, our point is that there exists sufficient energy in the nascent water dimer to cleave one of its O-H bonds, and it is such a process that we now consider.

To quantitatively characterize the heterolytic and homolytic energy profiles, we carried out *ab initio* calculations in which an O-H bond within the water dimer $\text{OH}_2 \cdots \text{OH}_2$ that is not involved in hydrogen bonding is elongated while relaxing all other geometrical degrees of freedom. In Fig. 7, we show the resulting diabatic energy profiles relating to heterolytic and homolytic bond cleavage for the three dielectric environments considered here.

The data in Figs. 1 and 7 combine to suggest that the following:

- for $\epsilon = 1$, PT happens where the steep energy drop occurs in Fig. 1(a), and the total energy involved in the steep drop (perhaps combined with thermal kinetic energy and the Coulomb energy drop associated with the ions' last displacement to approach the critical distance) produces a new O-H bond sufficiently "hot" to provide access to the homolytic dissociation pathway leading to $\text{H}_2\text{O} \cdots \text{OH} + \text{H}$;
- for $\epsilon = 2$ and $\epsilon = 78$, PT can happen where the steep drops occur in Figs. 1(b) and 1(c), respectively. However, the energy released in either of these PT energy drops (3.5 and 2.4 eV, respectively as seen in Figs. 1 and 7) does not produce the new O-H bond with enough energy to access the homolytic dissociation pathway as illustrated in Fig. 7. Thus, in these two cases, PT is not predicted to produce OH radicals and H atoms.

IV. SUMMARY

Our study leads us to conclude that electron transfer from OH^- to H_3O^+ to generate $\text{OH} + \text{H}_3\text{O}$ is feasible only if the microdroplet's environment produces little screening of the Coulomb attraction between the two ions once they are within ~ 10 Å of one another. Screening consistent with a dielectric constant of 2 or more would render this pathway extremely unlikely or impossible. Thus, if the screening is small enough, this electron transfer process could be a source for the OH radicals that were reported in Refs. 1 and 2, but we note that H atoms should be generated (by fragmentation of the fragile H_3O radical) in equal amounts, so experiments could be undertaken to search for them or for the products of their subsequent reaction as a test of this proposed mechanism.

We also considered proton transfer from H_3O^+ to OH^- to generate $(\text{H}_2\text{O})_2$ and found that the water dimer would be formed with its newly formed O-H bond quite elongated. For $\epsilon = 1$, the excess energy deposited in this elongated bond in the proton transfer step seems to be sufficient for the water dimer to undergo homolytic cleavage to form $\text{H}_2\text{O} \cdots \text{OH} + \text{H}$, again offering a route to OH radical and H atom formation. However, for $\epsilon = 2$ and $\epsilon = 78$, the excess energy realized in the proton transfer is considerably less and not sufficient to allow $\text{H}_2\text{O} \cdots \text{OH} + \text{H}$ to occur.

Finally, let us return to the issue of the role of strong local electric fields in the formation of OH radicals as discussed in Refs. 1 and 2. In those references, the authors suggest that an electric field in the $2\text{--}4 \times 10^7$ V/cm range acting over a distance of 5 Å would be sufficient to strip an electron off of an OH[−] ion to generate an OH radical. For example, a field of 4×10^7 V/cm moving an electron a distance of 5 Å would involve an energy of 2 eV, which is in excess of the 1.8 eV needed to detach an electron from a bare OH[−] anion. Reference 1 cites Ref. 3, noting that electric fields of this magnitude have been found in theoretical simulations of water, and Ref. 2 notes that in Ref. 4, electric fields of similar strength were found for those water molecules residing on microdroplet surfaces having two O–H bonds directed outward toward the vapor phase (so-called AA water molecules). It is known²⁶ that such AA molecules are especially capable of attracting and binding an excess electron, so it seems reasonable to suggest that it is such water molecules, when assisted by enhanced local electric fields, that are able to detach an electron from OH[−] to form OH. In this case, the electron should be found bound to a surface AA water molecule, thus suggesting an experimental test for this pathway. This kind of mechanism certainly remains a realistic possibility that our study does not reflect negatively on, but we do attempt to enhance it by suggesting where the electron detached from OH[−] goes (to an AA water molecule). We also want to point out that on pg. 678 of Ref. 25, the authors discuss the likelihood that a donor OH₂ molecule with one of its O–H bonds directed toward a surface AA molecule could enhance the AA molecule's electron binding strength (e.g., by forming a OH₂ · · · OH₂ structure having partial OH[−] · · · OH₃⁺ character).

In the two possibilities we suggest as alternative mechanisms, strong local electric fields also play key roles, but it is not the fields induced by the underlying water solvent molecules; instead, it is the strong field operative between an OH[−] anion and a H₃O⁺ cation residing on the surface. In the ET mechanism, once these two ions are within 5 Å of one another, which is where the ET is most likely to occur (see Fig. 1), their mutual Coulomb potential is $14.4/5 = 2.88$ eV for $\epsilon = 1$, more than sufficient to remove an electron from OH[−] to produce OH. We note that an energy of 2.88 eV would correspond to an electric field of 5.8×10^7 V/cm acting to move an electron from OH[−] anion's oxygen atom onto the H₃O⁺ cation when these two ions are separated by 5 Å.

In the PT mechanism, it is the strong inter-ion attraction that brings the two ions from ~ 10 Å into the region of the strong drop off in energy (see Fig. 1) where the O–H bond formed after the PT event is extremely elongated. In this case, for $\epsilon = 1$, the OH radical is generated by the nascent vibrationally hot water molecule undergoing homolytic cleavage.

AUTHOR DECLARATIONS

Conflict of Interest

The authors have no conflicts to disclose.

Author Contributions

Piotr Skurski: Conceptualization (supporting); Formal analysis (equal); Writing – original draft (equal). **Jack Simons:** Conceptualization (lead); Formal analysis (equal); Writing – original draft (equal).

DATA AVAILABILITY

The data that support the findings of this study are available within the article.

REFERENCES

- 1J. K. Lee, K. L. Walker, H. S. Han, J. Kang, F. B. Prinz, R. M. Waymouth, H. G. Nam, and R. N. Zare, "Spontaneous generation of hydrogen peroxide from aqueous microdroplets," *Proc. Natl. Acad. Sci. U. S. A.* **116**, 19294–19298 (2019).
- 2M. A. Mehrgardi, M. Mofidfar, and R. N. Zare, "Sprayed water microdroplets are able to generate hydrogen peroxide spontaneously," *J. Am. Chem. Soc.* **144**, 7606–7609 (2022).
- 3H. Hao, I. Leven, and T. Head-Gordon, "Can electric fields drive chemistry for an aqueous microdroplet?," *Nat. Commun.* **13**, 280 (2022).
- 4S. M. Kathmann, I. F. W. Kuo, and C. J. Mundy, "Electronic effects on the surface potential at the Vapor–Liquid interface of water," *J. Am. Chem. Soc.* **130**, 16556–16561 (2008).
- 5P. L. Geissler, C. Dellago, D. Chandler, J. Hutter, and M. Parrinello, "Autoionization in liquid water," *Science* **291**, 2121–2124 (2001).
- 6A. Hassanali, M. K. Prakash, H. Eshet, and M. Parrinello, "On the recombination of hydronium and hydroxide ions in water," *Proc. Natl. Acad. Sci. U. S. A.* **108**, 20410–20415 (2011).
- 7C. Möller and M. S. Plesset, "Note on an approximation treatment for many-electron systems," *Phys. Rev.* **46**, 618–622 (1934).
- 8M. Head-Gordon, J. A. Pople, and M. J. Frisch, "MP2 energy evaluation by direct methods," *Chem. Phys. Lett.* **153**, 503–506 (1988).
- 9M. J. Frisch, M. Head-Gordon, and J. A. Pople, "A direct MP2 gradient method," *Chem. Phys. Lett.* **166**, 275–280 (1990).
- 10R. A. Kendall, T. H. Dunning, Jr., and R. J. Harrison, "Electron affinities of the first-row atoms revisited. Systematic basis sets and wave functions," *J. Chem. Phys.* **96**, 6796–6806 (1992).
- 11M. W. Schmidt and K. Ruedenberg, "Effective convergence to complete orbital bases and to the atomic Hartree–Fock limit through systematic sequences of Gaussian primitives," *J. Chem. Phys.* **71**, 3951–3962 (1979).
- 12M. Gutowski and J. Simons, "Double-Rydberg anions: Ground-state electronic and geometric stabilities," *J. Chem. Phys.* **93**, 3874–3880 (1990).
- 13D. Hegarty and M. A. Robb, "Application of unitary group methods to configuration interaction calculations," *Mol. Phys.* **38**, 1795–1812 (1979).
- 14R. H. A. Eade and M. A. Robb, "Direct minimization in MC SCF theory. The quasi-Newton method," *Chem. Phys. Lett.* **83**, 362–368 (1981).
- 15H. B. Schlegel and M. A. Robb, "MC SCF gradient optimization of the H₂CO → H₂ + CO transition structure," *Chem. Phys. Lett.* **93**, 43–46 (1982).
- 16F. Bernardi, A. Bottoni, J. J. W. McDouall, M. A. Robb, and H. B. Schlegel, "MCSCF gradient calculation of transition structures in organic reactions," *Faraday Symp. Chem. Soc.* **19**, 137–147 (1984).
- 17M. J. Frisch, I. N. Ragazos, M. A. Robb, and H. Bernhard Schlegel, "An evaluation of three direct MC-SCF procedures," *Chem. Phys. Lett.* **189**, 524–528 (1992).
- 18N. Yamamoto, T. Vreven, M. A. Robb, M. J. Frisch, and H. Bernhard Schlegel, "A direct derivative MC-SCF procedure," *Chem. Phys. Lett.* **250**, 373–378 (1996).
- 19J. J. W. McDouall, K. Peasley, and M. A. Robb, "A simple MC SCF perturbation theory: Orthogonal valence bond Möller–Plesset 2 (OVBP2)," *Chem. Phys. Lett.* **148**, 183–189 (1988).
- 20S. Miertuš, E. Scrocco, and J. Tomasi, "Electrostatic interaction of a solute with a continuum. A direct utilization of AB initio molecular potentials for the prevision of solvent effects," *Chem. Phys.* **55**, 117–129 (1981).
- 21S. Miertuš and J. Tomasi, "Approximate evaluations of the electrostatic free energy and internal energy changes in solution processes," *Chem. Phys.* **65**, 239–245 (1982).
- 22M. Cossi, V. Barone, R. Cammi, and J. Tomasi, "Ab initio study of solvated molecules: A new implementation of the polarizable continuum model," *Chem. Phys. Lett.* **255**, 327–335 (1996).

²³M. J. Frisch, G. W. Trucks, H. B. Schlegel, G. E. Scuseria, M. A. Robb, J. R. Cheeseman, G. Scalmani, V. Barone, G. A. Petersson, H. Nakatsuji, X. Li, M. Caricato, A. V. Marenich, J. Bloino, B. G. Janesko, R. Gomperts, B. Mennucci, H. P. Hratchian, J. V. Ortiz, A. F. Izmaylov, J. L. Sonnenberg, D. Williams-Young, F. Ding, F. Lipparini, F. Egidi, J. Goings, B. Peng, A. Petrone, T. Henderson, D. Ranasinghe, V. G. Zakrzewski, J. Gao, N. Rega, G. Zheng, W. Liang, M. Hada, M. Ehara, K. Toyota, R. Fukuda, J. Hasegawa, M. Ishida, T. Nakajima, Y. Honda, O. Kitao, H. Nakai, T. Vreven, K. Throssell, J. A. Montgomery, Jr., J. E. Peralta, F. Ogliaro, M. J. Bearpark, J. J. Heyd, E. N. Brothers, K. N. Kudin, V. N. Staroverov, T. A. Keith, R. Kobayashi, J. Normand, K. Raghavachari, A. P. Rendell, J. C. Burant, S. S. Iyengar, J. Tomasi, M. Cossi, J. M. Millam, M. Klene, C. Adamo,

R. Cammi, J. W. Ochterski, R. L. Martin, K. Morokuma, O. Farkas, J. B. Foresman, and D. J. Fox, *Gaussian 16, Revision C.01*, Gaussian, Inc., Wallingford CT, 2016.

²⁴C. Gonzalez and H. B. Schlegel, "An improved algorithm for reaction path following," *J. Chem. Phys.* **90**, 2154–2161 (1989).

²⁵A nice modern treatment can be found in E. P. Glasbrenner and W. P. Schleich, "The Landau–Zener formula made simple," *J. Phys. B: At., Mol. Opt. Phys.* **56**(10), 104001 (2023).

²⁶N. I. Hammer, J.-W. Shin, J. M. Headrick, E. G. Diken, J. R. Roscioli, G. H. Weddle, and M. A. Johnson, "How do small water clusters bind an excess electron?," *Science* **306**, 675–679 (2004).